# Interlaced Kalman Filtering of 3-D Angular Motion Based on Euler's Nonlinear Equations

**MARCELO C. ALGRAIN**, Senior Member, IEEE
University of Nebraska-Lincoln

**JAFAR SANIIE**, Senior Member, IEEE
Illinois Institute of Technology

**A novel Kalman filtering technique is presented that reduces the mean-square-error (MSE) between three-dimensional (3-D) actual angular velocity values and estimated ones by an order of magnitude (when compared with the MSE resulting from direct measurements) even under extremely low signal-to-noise ratio conditions. The filtering problem is nonlinear in nature because the dynamics of 3-D angular motion are described by Euler's equations. This nonlinear set of differential equations state that the angular acceleration in one axis is proportional to the torque applied to that axis, and to the products of angular velocity components in the other two axes of rotation. Instead of using extended Kalman filtering techniques to solve this complex problem, the authors developed a new approach where the nonlinear Euler's model is decomposed into two pseudolinear models (primary and secondary). The first model describes the time progression of the state vector containing the linear terms, while the other characterizes the propagation of the state vector containing the nonlinearities. This makes it possible to run two interlaced discrete-linear Kalman filters simultaneously. One filter estimates the values of the state vector containing the linear terms, while the other estimates the values of the state vector containing the nonlinear terms in the system. These estimates are then recombined, solving the nonlinear estimation process without linearizing the system. Thus, the new approach takes advantage of the simplicity, computational efficiency and higher convergence speed of the linear Kalman filter form, and it overcomes many of the drawbacks typical of conventional extended Kalman filtering techniques. The high performance and effectiveness of this method is demonstrated through a computer simulation case study.**

Manuscript received August 20, 1992; revised December 24, 1992 and June 25, 1993.

IEEE Log No. T-AES/30/1/13054.

Authors' addresses: M. C. Algrain, Electrical Engineering Dept., University of Nebraska-Lincoln, Lincoln, NE 68588-0511; J. Saniie, Electrical and Computer Engineering Dept., Illinois Institute of Technology, Chicago, IL 60616.



## INTRODUCTION

Among the successful applications of Kalman filtering are geosynchronous satellite orbit determination systems [1–2], tracking systems [3–5], and integrated navigation systems [6–7]. A typical aircraft integrated navigation system consists of an Inertial Navigation System (INS) combined with independent navigation measurements from a Doppler radar, Global Positioning System (GPS), or Loran receiver. The INS provides very accurate navigation data, over short intervals, based on the outputs of three orthogonally mounted rate-gyros and three orthogonally mounted linear accelerometers, which measure aircraft body motion [8]. A GPS typically uses positional information of at least four satellites to derive the range vectors rates of change (from aircraft to satellites), determining vehicle attitude and its rate of change. The integration of two or more independent navigators can be performed using extended Kalman filtering techniques [9]. This produces more accurate navigation data than from either navigator individually. Elaborate models have been proposed to implement integrated navigation systems and to obtain proper alignment between them. In a recent paper [10], a 63 by 63 transition matrix was used (consisting of platform rate, Earth rate, and direction cosines) in the development of large-dimension Kalman filters for the calibration and alignments of complex inertial guidance systems. Needless to say that such Kalman filters are overwhelming in size.

The wide applicability of Kalman filtering is largely due to the fact that the method is extendable to nonlinear systems; however, extended Kalman filtering processes are not generally optimal. The method is often used because no other general technique has yet been found that works better for nonlinear problems. The extension of the linear Kalman filter form to nonlinear systems involves, at one point or another, a linearization process. In the case of the linearized Kalman filter (LKF), the linearization is carried along a precomputed trajectory. Similarly, the extended Kalman filter (EKF) uses a linearization along the estimated trajectory of the filter. The accuracy of these estimation algorithms depends on how closely the actual trajectory is to the nominal one, and significant deviations may lead to filter divergence. Also, the success of these techniques is largely dependent on the accuracy of the linearization method used. In some cases, the linearization can be accomplished through perturbation techniques or by truncated Taylor series expansions; in other cases, a piecewise-linear approach may be necessary to preserve linearization accuracy, and to avoid filter divergence. However, in many cases, the system dynamics do not lend themselves to practical linear characterizations, and very complex models are required to represent these systems.

The Kalman filtering of three-dimensional (3-D) gyroscopic measurements follows naturally in context with the preceding applications. The 3-D nonlinear angular motion of a body is described by Euler's equations. Euler's equations state that the angular acceleration in one axis is proportional to the product of angular velocities in the other two axes orthogonal to the first, and also proportional to the torque applied to the first axis [11]. Linearizing these equations is no trivial task. One could brute force the linearization process and utilize state augmentation methods until a satisfactory linear approximation for Euler's equations is obtained. Alternatively, one could take advantage of relationships between linear accelerations and products of angular velocity components, and avoid complex and sometimes inaccurate linearization processes. These relationships allow to obtain the product of two orthogonal angular velocity components from a linear combination of four translational accelerations [12]. This permits to redefine Euler's model in terms of angular velocities and linear accelerations, and to decompose a single nonlinear model into two pseudolinear models.

The novelty of the approach presented here consists in the replacement of a nonlinear model with two pseudolinear models (one uses angular velocities and the other contains linear accelerations), and the utilization of two interlaced linear Kalman filters running simultaneously. The first filter estimates orthogonal angular velocity components (roll, pitch, and yaw rates), and the second filter estimates linearly combined translational accelerations (which is equivalent to estimating the products between two orthogonal angular velocity components). The output of the first Kalman filter feeds into the second, and the output of the second feeds into the first filter, forming the interlaced Kalman filter (IKF) method. This approach solves the nonlinear 3-D angular velocity estimation problem, without requiring the linearization of Euler's equations. Furthermore, the IKF method takes advantage of the simplicity, computational efficiency, and higher convergence speed of the discrete-linear form; and it overcomes some of the drawbacks of conventional extended Kalman filtering techniques [13], since the system is never linearized.

The fundamental differences between the IKF method and the EKF (or the LKF) approach are as follows. In the EKF and LKF methods, the system model is linearized along a nominal trajectory (estimated or precomputed). The accuracy of the filter depends on how close the actual trajectory is to the nominal one, and significant deviations lead to filter divergence. On the other hand, the IKF method does not use a linearized system model. Instead, the system is split into linear and nonlinear terms. The linear terms are redefined as a primary state vector, and nonlinear terms are redefined as a secondary state vector. This allows to form two pseudolinear models based on the primary and secondary state vectors. One model describes the time progression of the primary state vector (containing the linear terms), while the other characterizes the propagation in time of the secondary state vector (containing the nonlinear terms). Even though the secondary state vector contains the system nonlinearities, the secondary model is linear in terms of the secondary state vector, and a linear Kalman filter can be used for estimation purposes. Therefore, it is feasible to run two interlaced discrete-linear Kalman filters (simultaneously), one estimates linear terms, and the other estimates the nonlinear terms, without linearizing the systems at any point. For this reason, the IKF method can be applied to other nonlinear systems, just by decomposing the system model in linear and nonlinear terms, filtering them separately, and recombining the individual estimates through the proper nonlinear operator, afterwards.

## THE IKF METHOD FOR 3-D ANGULAR MOTION

The Kalman filter is a linear minimum-error-variance recursive estimation technique [14]. Its ability to produce more accurate values of measured variables is attributed to the use of statistical information about the process that generated those variables, as well as statistical information about the noise in the measurements of those variables, in the computation of the estimates [15]. Furthermore, the filter incorporates knowledge about the system itself through a model of its dynamical characteristics. In the case of 3-D angular motion, the system dynamics are described by Euler's equations of motion. Expressing that motion along the body's principal axes of inertia leads to the following expressions [16]:

$$\dot{W}_x = (I_{YY} - I_{ZZ})/I_{XX}(W_Y W_Z) + I_{XX}^{-1} M_X \quad (1a)$$

$$\dot{W}_Y = (I_{ZZ} - I_{XX})/I_{YY}(W_X W_Z) + I_{YY}^{-1} M_Y \quad (1b)$$

$$\dot{W}_Z = (I_{XX} - I_{YY})/I_{ZZ}(W_X W_Y) + I_{ZZ}^{-1} M_Z \quad (1c)$$

where

| | |
|---|---|
| $I_{XX}$ | Principal moment of inertia about roll axis. |
| $I_{YY}$ | Principal moment of inertia about pitch axis. |
| $I_{ZZ}$ | Principal moment of inertia about yaw axis. |
| $M_X$ | Torque applied to roll axis. |
| $M_Y$ | Torque applied to pitch axis. |
| $M_Z$ | Torque applied to yaw axis. |
| $W_X$ | Body angular velocity along roll axis. |
| $W_Y$ | Body angular velocity along pitch axis. |
| $W_Z$ | Body angular velocity along yaw axis. |
| $\dot{W}_X$ | Body angular acceleration along roll axis. |
| $\dot{W}_Y$ | Body angular acceleration along pitch axis. |
| $\dot{W}_Z$ | Body angular acceleration along yaw axis. |

Equations (1a)–(1c) provide a set of nonlinear differential equations that completely defines

the angular motion of a rigid body in 3-D space. To use them as the system model for the discrete Kalman filter they need to be expressed as difference equations. This can be accomplished (for sufficiently small time intervals) by approximating an angular acceleration with the first forward difference between consecutive angular velocities (more accurate approximations are possible, but may lead to more complicated expressions) as follows:

$$\dot{W}(n) = (W(n+1) - W(n))/T \tag{2}$$

where

| | |
|---|---|
| $\dot{W}(n)$ | Angular acceleration. |
| $W(n+1)$ | Angular velocity at time index "$n+1$." |
| $W(n)$ | Angular velocity at time index "$n$." |
| $T$ | Incremental time step. |

Substituting (2) into (1a)–(1c), and after some manipulations, the following state-space representation for the discrete-time progression of 3-D angular velocities is obtained

$$X_W(n+1) = X_W(n) + A(n)X_A(n) + B(n)U_W(n) \tag{3}$$

where

$$X_W = [W_X W_Y W_Z]^T$$

$$X_A = [A_X A_Y A_Z]^T = [W_Y W_Z \quad W_X W_Z \quad W_X W_Y]^T$$

$$U_W = [M_X M_Y M_Z]^T$$

and the matrices $A$ and $B$ are defined as follows:

$$A(n) = \begin{bmatrix} T(I_{YY} - I_{ZZ})I_{XX}^{-1} & 0 & 0 \\ 0 & T(I_{ZZ} - I_{XX})I_{YY}^{-1} & 0 \\ 0 & 0 & T(I_{ZZ} - I_{YY})I_{ZZ}^{-1} \end{bmatrix};$$

$$B(n) = \begin{bmatrix} TI_{XX}^{-1} & 0 & 0 \\ 0 & TI_{YY}^{-1} & 0 \\ 0 & 0 & TI_{ZZ}^{-1} \end{bmatrix}.$$

To complete the model, the means for propagating the products of angular velocity components need to be devised. These products were previously defined in the vector form as follows:

$$X_A = [A_X \quad A_Y \quad A_Z]^T = [W_Y W_Z \quad W_X W_Z \quad W_X W_Y]^T. \tag{4}$$

Differentiating each element in (4) leads to the following relationships:

$$\dot{A}_X = W_Z \dot{W}_Y + W_Y \dot{W}_Z \tag{5a}$$

$$\dot{A}_Y = W_Z \dot{W}_X + W_X \dot{W}_Z \tag{5b}$$

$$\dot{A}_Z = W_Y \dot{W}_X + W_X \dot{W}_Y. \tag{5c}$$

Using first difference approximations for continuous time derivatives in (5a)–(5c) (forward difference on left-hand side, and backward difference on the right-hand side of the equations), leads to the following state-space representation for the progression in time of products of orthogonal angular velocity components:

$$X_A(n+1) = X_A(n) + F[X_W(n), X_W(n-1)] + U_A(n) \tag{6}$$

where

$U_A$ = an approximation error term that forces the equality to hold

$$F[X_W(n), X_W(n-1)] = [F_X \quad F_Y \quad F_Z]^T$$

$$F_X = [W_Y(n) - W_Y(n-1)]W_Z(n) + [W_Z(n) - W_Z(n-1)]W_Y(n)$$

$$F_Y = [W_X(n) - W_X(n-1)]W_Z(n) + [W_Z(n) - W_Z(n-1)]W_X(n)$$

$$F_Z = [W_X(n) - W_X(n-1)]W_Y(n) + [W_Y(n) - W_Y(n-1)]W_X(n).$$

Equation (6) gives a linear model for the propagation of the state vector $X_A$. This model contains a nonlinear function of the state vector $X_W$, but it is linear in terms of the state vector $X_A$, thus complying with the linearity criteria for that state-variable. This is the key consideration in developing a pseudolinear Euler's equivalent model. Therefore, (3) and (6) provide a discrete-time Euler's equivalent model which allows estimation of 3-D velocities using two discrete-linear Kalman filters running simultaneously. The first filter estimates orthogonal angular velocity components, and the second estimates their products (taken two at a time). The result is an optimal filtering method, which allows estimation of 3-D angular velocities in a robust, efficient, and accurate manner [17]. The multivariable IKF process is depicted in Fig. 1, where $K_W$ is the matrix containing the Kalman gains for angular velocity components, $K_A$ is the matrix containing the Kalman gains for products of angular velocity components, $X_W(n)$ and $X_A(n)$ are the estimated values of 3-D angular velocity components and their products (at time index $n$), respectively, and $X_W(n \mid n-1)$ and $X_A(n \mid n-1)$ are the predicted values based on the $n-1$ measurements.

The IKF method makes it possible to treat angular velocities and combined linear accelerations as separate states. Thus, the two states need to be measured individually. These measurements can be obtained from an arrangement of 3 orthogonal gyros and 9 linear accelerometers. The linearly combined accelerometer outputs provide independent measurements for products of angular velocity

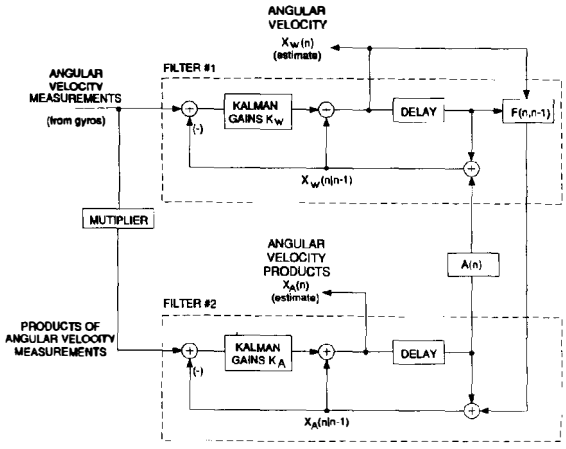


Fig. 1. Interlaced Kalman filter block diagram.

components. However, because of the equivalence between products of angular velocities and combined linear accelerations, measurements for combined linear accelerations can also be obtained algebraically by direct multiplication of the proper angular velocity measurements. This eliminates the need for the 9 linear accelerometers, considerably reducing the complexity of the measurement scheme required by the IKF process estimating 3-D angular velocities.

## IKF PERFORMANCE EVALUATION

The performance of the IKF method estimating the 3-D angular velocity of a body is evaluated in this section through a computer simulation case study. The simulation was implemented using the ACSL software package from Mitchell and Gauthier, Associates, Inc. The actual angular velocity components were obtained by solving (1a)–(1c) (Euler's equations) numerically. The integration algorithm used was a forth-order Runge-Kutta. The simulation incremental time step was 0.01 s. The body was assumed to be a rigid body having the following normalized principal moments of inertia: roll axis, $I_{XX} = 1.00$; pitch axis, $I_{YY} = 0.75$; yaw axis, $I_{ZZ} = 0.50$.

The torque disturbances $M_X$, $M_Y$, and $M_Z$ (applied to each of the orthogonal axes) have Gaussian distribution with zero mean and variance of one. Also, to be able to visualize the time plots of the torque disturbances, and of the resulting angular velocities, the torque signal bandwidth is limited to 1 Hz. This is done for illustration purposes only, and it is not a limitation of the technique. The torque disturbances define the vector $U_W = [M_X M_Y M_Z]^T$ as the random forcing function applied to the body, causing it to rotate at angular velocity $W = [W_X W_Y W_Z]^T$.

Fig. 2(a) shows a time plot of the random torque disturbance $M_X$ applied to the $X$ axis (roll axis) of the body, and Fig. 2(b) shows the resulting roll angular

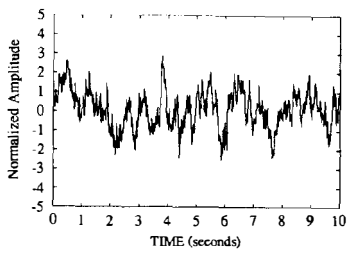


Fig. 2(a). Roll torque disturbance ($M_X$).

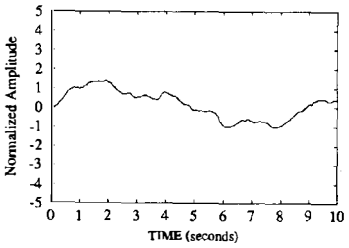


Fig. 2(b). Actual roll rate ($W_X$).

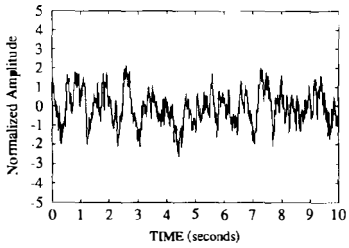


Fig. 3(a). Pitch torque disturbance ($M_Y$).

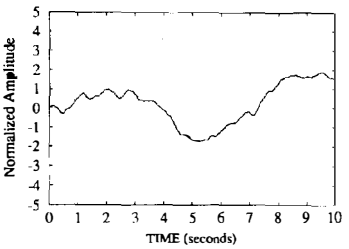


Fig. 3(b). Actual pitch rate ($W_Y$).

rate $W_X$. Similarly, Figs. 3(a) and 4(a) show the torque disturbances $M_Y$ and $M_Z$ applied to the $Y$ and $Z$ axes (pitch and yaw axes, respectively), and Figs. 3(b) and 4(b) show the resulting angular velocities $W_Y$ and $W_Z$ (pitch and yaw rates, respectively). All variables are given in normalized form in order to generalize the estimation case.

The measured angular velocity components (obtained from 3 orthogonal gyroscopes) are shown in Figs. 5(a), 6(a), and 7(a), respectively. The noise components in each of these measurements also have Gaussian distribution, zero mean and variance of one (low signal-to-noise ratio condition). Figs. 5(b), 6(b),

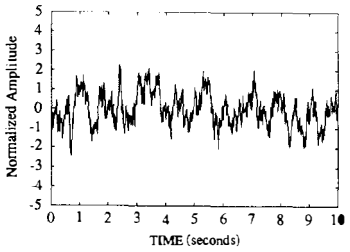


Fig. 4(a). Yaw torque disturbance ($M_Z$).

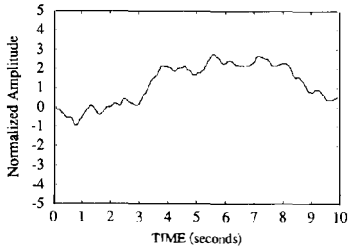


Fig. 4(b). Actual yaw rate ($W_Z$).

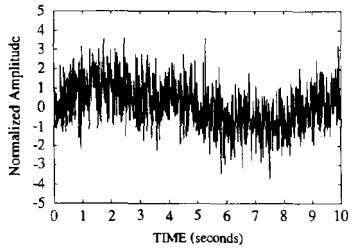


Fig. 5(a). Roll rate ($W_X$) measurement.

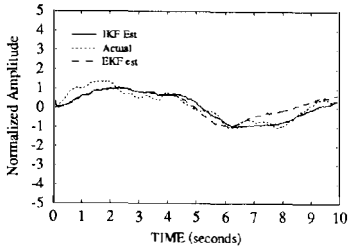


Fig. 5(b). Actual and estimated $W_X$

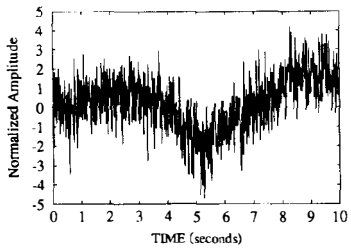


Fig. 6(a). Pitch rate ($W_Y$) measurement.

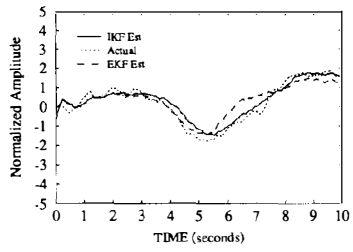


Fig 6(b). Actual and estimated $W_Y$.

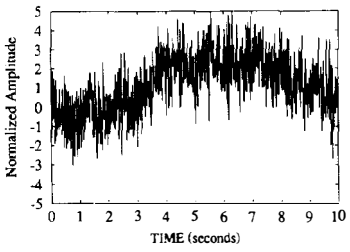


Fig. 7(a). Yaw rate ($W_Z$) measurement.

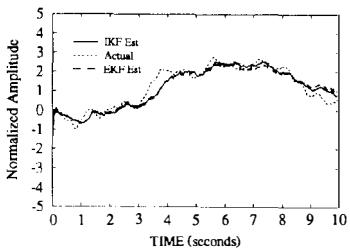


Fig. 7(b). Actual and estimated $W_Z$.

and 7(b) show the IKF angular velocity estimates in the roll, pitch, and yaw axes, respectively. For comparison purposes, the actual velocity values $W_X$, $W_Y$, and $W_Z$ are shown as dotted lines, and the EKF estimates are shown as dashed lines.

Comparing the values of the actual 3-D angular velocity $W$, its estimate $X_W$ and its measurement $Z_W$ (see Figs. 5–7), it is clear that the IKF technique provides outstanding 3-D angular velocity estimates in spite of the very low signal-to-noise ratio condition imposed. The reader is referred to [17] for a more complete assessment on IKF estimation accuracy under a variety of conditions and scenarios.

To further demonstrate the improvements IKF estimates offer over the EKF estimates and the raw gyroscope measurements, Fig. 8(a), 9(a), and 10(a) show time plots of the measurement noise in the roll, pitch, and yaw axes, respectively, while Figs. 8(b), 9(b), and 10(b) show time plots of estimation errors for angular velocity components in the roll, pitch, and yaw axes, respectively. It is clear from these figures that the EKF estimation errors are significantly lower than those errors (noise) present in the measurements and those yielded by the EKF method. This is further manifested when the respective estimation mean-square-errors (MSEs) are compared (see

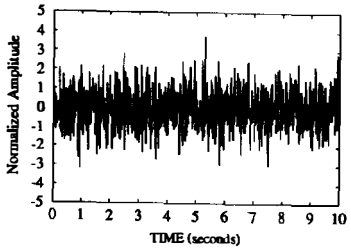


Fig. 8(a). Roll rate measurement noise.

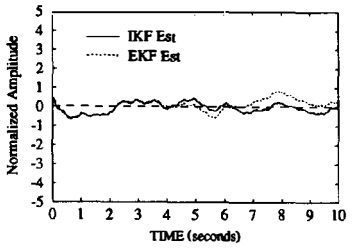


Fig. 8(b). Roll rate estimation error.

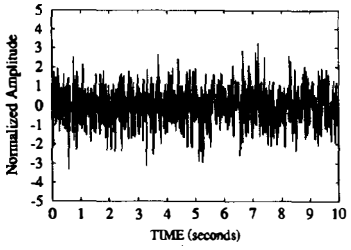


Fig. 9(a). Pitch rate measurement noise.

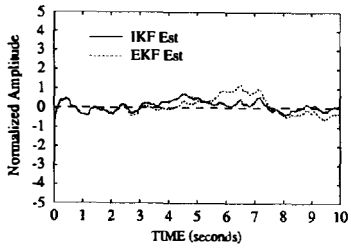


Fig. 9(b). Pitch rate estimation error.

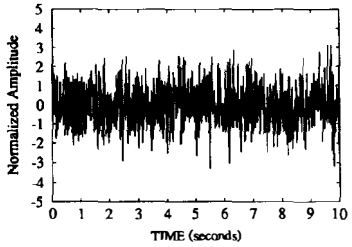


Fig. 10(a). Yaw rate measurement noise.

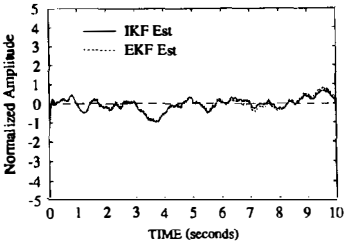


Fig. 10(b). Yaw rate estimation error.

TABLE I
MSE of Velocity Estimates

| Estimation Case | IKF | EKF | Measured |
|---|---|---|---|
| Roll Axis | 0.0751 | 0.1311 | 0.9981 |
| Pitch Axis | 0.0751 | 0.1921 | 0.9122 |
| Yaw Axis | 0.1106 | 0.1211 | 1.0492 |

TABLE II
Mean Velocity Estimation Errors

| Estimation Case | IKF | EKF | Measured |
|---|---|---|---|
| Roll Axis | −0.0425 | 0.0642 | −0.0108 |
| Pitch Axis | 0.0615 | 0.0845 | 0.0081 |
| Yaw Axis | −0.0226 | −0.0345 | −0.0252 |

Table I). In all cases, the MSE for the IKF estimates are considerably smaller than the MSE for the EKF estimates, and it is over one order of magnitude smaller than the MSE for the measurements. In addition, Table II provides the means of the angular velocity estimation errors for each axis, as well as for the measurement noises. These means are nearly zero, attesting for the unbiasedness of the IKF method.

The preceding analysis addresses the IKF estimation accuracy for 3-D angular velocities. To complete it, the accuracy of the estimates for the products of angular velocity components needs to be evaluated. The components of the measured angular velocity product $Z_A$ (obtained from gyroscope measurements) are shown in Figs. 11(a), 12(a), and 13(a). Figs. 11(b), 12(b), and 13(b) show the IKF estimate $X_A$ for products of angular velocity components. The actual velocity products are also plotted for comparison purposes (shown as dashed lines). In addition, Figs. 14(a), 15(a), and 16(a) show time plots of the measurement noise for each of the angular velocity products, while Figs. 14(b), 15(b), and 16(b) show time plots of the estimation errors for each of the angular velocity products.

Comparing the values of the actual products of angular velocity components, the estimated values and the measured ones (see Figs. 11–13), it is evident that the IKF technique provides excellent estimates of products between angular velocity components, even under the very low signal-to-noise ratio condition imposed. Moreover, Figs. 14–16 clearly indicate that the estimation errors are significantly lower than

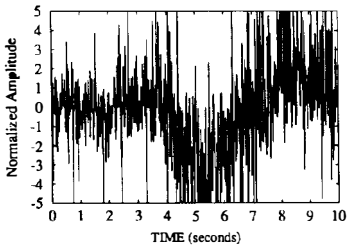


Fig. 11(a). Pitch-yaw product ($A_X$) measurement.

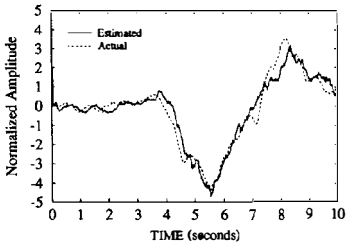


Fig. 11(b). Actual and estimated $A_X$.

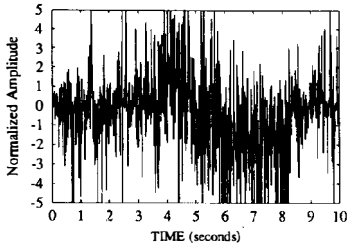


Fig. 12(a). Roll-yaw product ($A_Y$) measurement.

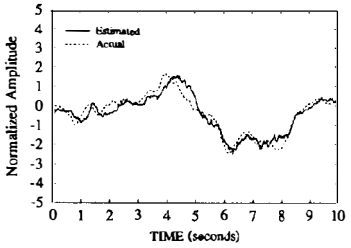


Fig. 12(b). Actual and estimated $A_Y$.

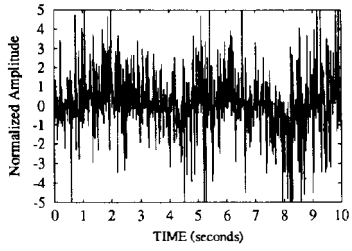


Fig. 13(a). Roll-pitch product ($A_Z$) measurement.

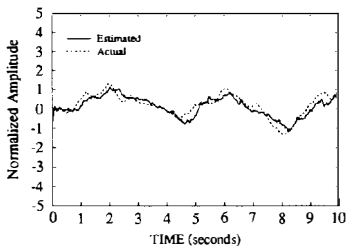


Fig. 13(b). Actual and estimated $A_Z$.

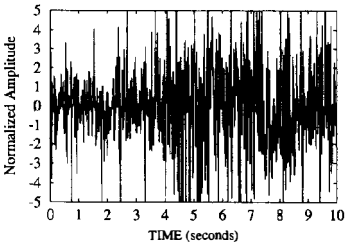


Fig. 14(a). Pitch-yaw product noise.

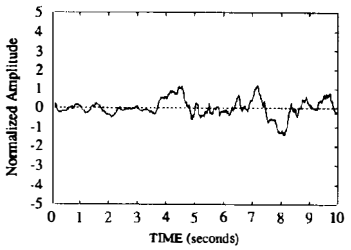


Fig. 14(b). Pitch-yaw product estimation error.

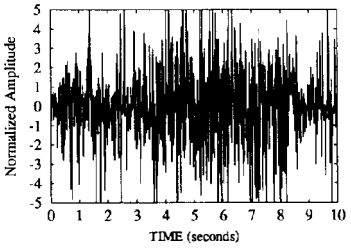


Fig. 15(a). Roll-yaw product noise.

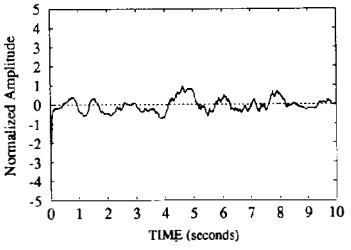


Fig. 15(b). Roll-yaw product estimation error.

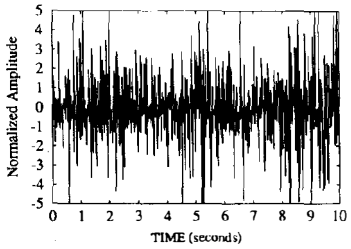


Fig. 16(a). Roll-pitch product noise.

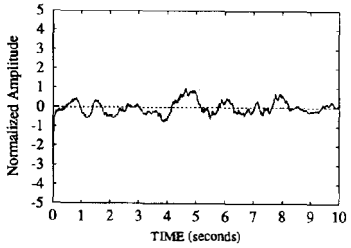


Fig. 16(b). Roll-pitch product estimation error.

TABLE III
MSE of Velocity Product Estimates

| Estimation Case | IKF | Measured |
|---|---|---|
| Pitch · Yaw Product | 0.2736 | 6.4145 |
| Roll · Yaw Product | 0.0704 | 4.8801 |
| Roll · Pitch Product | 0.0792 | 3.1131 |

TABLE IV
Mean Velocity Product Estimation Errors

| Estimation Case | IKF | Measured |
|---|---|---|
| Pitch · Yaw Product | 0.0511 | 0.0268 |
| Roll · Yaw Product | 0.0035 | −0.0093 |
| Roll · Pitch Product | 0.0879 | 0.0536 |

those errors in the direct measurements (noise). Also, the MSEs provided in Table III demonstrate high estimation accuracy. In all cases, the MSEs of the IKF are about one order of magnitude smaller than the MSEs for measured values. In addition, Table IV provides the angular velocity product estimation error means, and the noise means for the corresponding gyroscope measurements. From these values, it can be concluded that the IKF estimates of products between angular velocity components are unbiased (the estimation error means are nearly zero).

The predominant steady-state Kalman gains for the IKF technique are given in Table V. The gains for angular velocities are different (for each of the axes), because the moments of inertia (in each of those axes) are different. Conversely, the steady-state Kalman gains for any product combination of two angular velocity components are equal to each other. This is due to the symmetry in (5a)–(5c).

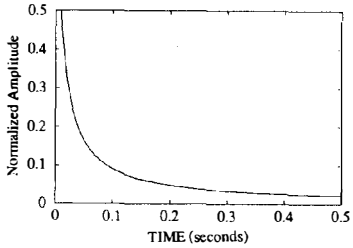


Fig. 17(a). Kalman gain $K_{Wx}$.

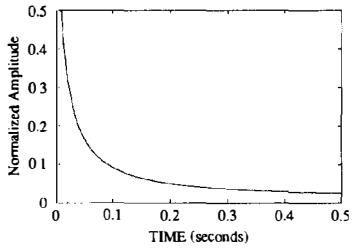


Fig. 17(b). Kalman gain $K_{Ax}$.

TABLE V
Steady-State IKF Gains

| State-Variable | Kalman Gain |
|---|---|
| $W_X$ | 0.00995 |
| $W_Y$ | 0.01324 |
| $W_Z$ | 0.01980 |
| $A_X$ | 0.01569 |
| $A_Y$ | 0.01569 |
| $A_Z$ | 0.01569 |

Figs. 17(a), 18(a), and 19(a) show the angular velocity Kalman gains $K_{Wx}$, $K_{Wy}$, and $K_{Wz}$, respectively, versus time. The matrix $K_W$ is a diagonal matrix, i.e., nondiagonal elements are zero, and therefore not shown. Figs. 17(b), 18(b), and 19(b) show, respectively, the Kalman gains ($K_{Ax}$, $K_{Ay}$, and $K_{Az}$) for products of angular velocity components versus time ($K_A$ is also a diagonal matrix). For both Kalman gain matrices, the gains reach near steady-state values within 10 time steps (0.1 s) indicating the fast convergence speed of the IKF method.

In short, the results from this computer simulation clearly demonstrate the advantages of determining 3-D angular velocities using the IKF technique. Even if there is some uncertainty about the exact values of these inertias, the IKF estimates are not seriously affected as long as the errors are not severe [17]. This is important since moments of inertia could change as the parameters within the body could change due to various factors. If the significance of these factors become large, it may be necessary to correct the moments of inertia accordingly, so that good estimation accuracy is preserved. Furthermore, the

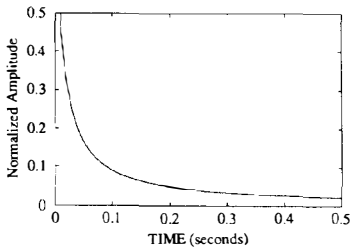


Fig. 18(a). Kalman gain $K_{Wy}$.

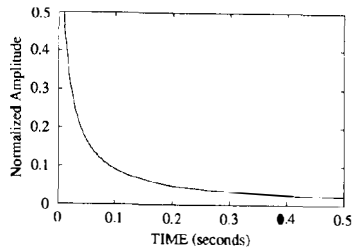


Fig. 18(b). Kalman gain $K_{Ay}$.

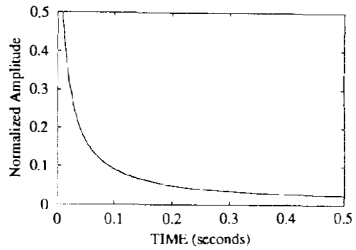


Fig. 19(a). Kalman gain $K_{Wz}$.

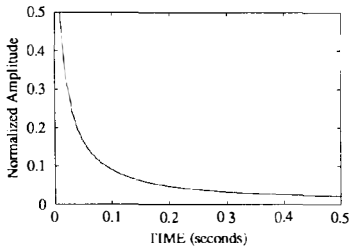


Fig. 19(b). Kalman gain $K_{Az}$.

IKF approach effectively supresses gyroscope noise, since it provides far more accurate angular rates than gyroscopes, by themselves, could. This would permit a relaxation in gyroscope noise specifications which is highly desirable in practice, since it could lead to substantial savings.

## SUMMARY AND CONCLUSIONS

The importance of 3-D angular motion estimation is attested by the many critical applications where body angular motion needs to be accurately known. Among these applications are strap-down inertial navigation, space vehicle attitude and orbit control, fine pointing and tracking, inertial stabilization of platforms, and long-range reconnaissance. Angular velocities are commonly measured using rate-gyros. These instruments are particularly sensitive to spurious torques. Random or unpredicted variations of these torques introduce measurement errors. The magnitude and distribution of these errors establish the noise level and define measurement uncertainties. Optimal estimators can be used to minimize these uncertainties.

This paper presents a novel method to estimate 3-D angular motion based on noisy gyroscopic measurements. The estimation problem is nonlinear since the dynamics of 3-D angular motion are described by Euler's equations. Instead of using complex extended Kalman filtering techniques to solve this problem, the IKF method is developed where the nonlinear Euler's model is decomposed into two pseudolinear models. This makes it possible to run two interlaced linear Kalman filters. This technique takes advantage of the simplicity, computational efficiency, and higher convergence speed of the linear form. The effectiveness of the IKF method is evaluated through a computer simulation. The simulation demonstrates that the IKF method yields outstanding 3-D angular velocity estimates, gives signal-to-noise ratio improvements of about 20 dB, even under very low signal-to-noise ratio conditions (near 0 dB), outperforming the estimates obtained using the extended Kalman filter.

The IKF method can easily be applied to other nonlinear systems by redefining the nonlinear terms as part of an auxiliary vector. This effectively decomposes a single nonlinear model into a primary discrete-time linear model and an auxiliary one. The primary model describes the time progression of the state variables containing the linear terms, while the other characterizes the propagation in time of the auxiliary state vector containing the nonlinearities. This approach makes it possible to run two interlaced discrete-linear Kalman filters, solving a generic nonlinear estimation problem without linearizing the system. The advantages of this methodology are simplicity and high computational and convergence speeds. In addition, the new approach allows us to overcome some of the drawbacks of extended Kalman filtering techniques which tend to be system dependent, and are afflicted by divergence tendencies.

## ACKNOWLEDGMENT

The authors wish to thank Marjorie Bisbee, from the Engineering Research Centers Office at the University of Nebraska-Lincoln, for her fabulous and prompt work in the preparation of all the figures appearing in this paper.

REFERENCES


[1] Steffan, K. F. (1963)
*Orbital Guidance and Control of Aerospace Vehicles.*
New York: McGraw-Hill, 1963.

[2] Brogan, W. L., and LeMay, J. L. (1968)
Autonomous Orbit Determination of Synchronous Altitude.
In *Proceedings of the AAS/AIAA Astrodynamics Specialist Conference*, Sept. 1968, 345–350.

[3] Song, T. L., Ahn, J. Y., and Park, C. (1988)
Suboptimal filter design with pseudo-measurements for target tracking.
*IEEE Transactions on Aerospace and Electronic Systems*, **24** (Jan. 1988), 51–58.

[4] Spingarn, K. (1987)
Passive position location estimation using the extended Kalman filter.
*IEEE Transactions on Aerospace and Electronic Systems*, **AES-23** (July 1987), 617–628.

[5] Bogler, P. L. (1987)
Tracking a maneuvering target using input estimation.
*IEEE Transactions on Aerospace and Electronic Systems*, **AES-23** (May 1987), 527–534.

[6] Brown, R. G. (1972)
Integrated navigation system and Kalman filtering: A perspective.
*Journal of the Institute of Navigation*, **19**, 4 (Winter 1972–1973), 355–362.

[7] Schmidt, S. F., Weinberg, J. S., and Lukesh, J. S. (1968)
Case study of Kalman filtering in the C-5 aircraft navigation system.
Case Studies in Systems Control, University of Michigan, June, 1968.

[8] Kayton, M. (1990)
*Navigation: Land, Sea, Air, and Space.*
New York: IEEE Press, 1990.

[9] Brockstein, A. J. (1976)
GPS-Kalman-augmented inertial navigation system performance.
*NAECON'76 Record*, May 1976, 864–871.

[10] Grewal, S. M., Henderson, V. D., and Miyasako, R. S. (1991)
Application of Kalman filtering to the calibration and alignment of inertial navigation systems.
*IEEE Transactions on Automatic Control* (Jan. 1991), 4–13.

[11] Beer, F., and Johnson, E. (1984)
*Vector Mechanics for Engineers* (4th ed.).
New York: McGraw-Hill, 1984.

[12] Algrain, M. C., and Saniie, J. (1991)
Estimation of 3-D angular motion using gyroscopes and linear accelerometers.
*IEEE Transactions on Aerospace and Electronic Systems*, **27**, 6 (Nov. 1991), 910-920.

[13] Sorenson, H. W. (1985)
*Kalman Filtering: Theory and Applications.*
New York: IEEE Press, 1985.

[14] Chui, C. K., and Chen, G. (1987)
*Kalman Filtering with Real-Time Applications.*
New York: Springer-Verlag, 1987.

[15] Brown, R. G., and Hwang, P. (1991)
*Introduction to Random Signals and Applied Kalman Filtering.*
New York: Wiley, 1991.

[16] D'Souza, A. F., and Garg, V. K. (1984)
*Advanced Dynamics, Modeling and Analysis.*
Englewood Cliffs, NJ: Prentice-Hall, 1984.

[17] Algrain, M. C. (1991)
On the optimal estimation of 3-D angular motion.
Ph.D. dissertation, Illinois Institute of Technology, Chicago, May 1991.

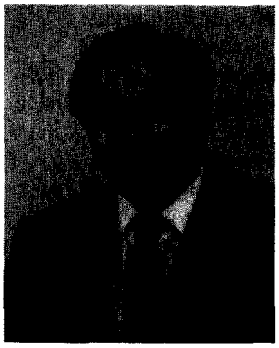

**Marcelo C. Algrain** (S'89—M'91—SM'93) was born in Rosario, Argentina, in 1957. He received a B.S.M.E. in 1980 and an M.S.E.E. in 1981, both from Wright State University, Dayton, OH, and in 1991 the Ph.D. in electrical engineering from the Illinois Institute of Technology, Chicago.

Since 1991 he has been an Assistant Professor at the University of Nebraska-Lincoln. From 1989 to 1991, he held the position of Engineering Specialist at Recon/Optical, Inc., where he performed analyses on stabilization and control systems for high-resolution reconnaissance systems. From 1984 to 1989, he was with Borg-Warner Research, developing control system prototypes for a variety of automotive and industrial products. Prior to Borg-Warner, he was with Babcock & Wilcox, designing process control systems for nuclear power plants. His research interests are in stabilization, pointing and tracking systems, and in stochastic, optimal and adaptive controls.

Dr. Algrain is a member of the Institute of Electrical and Electronic Engineers, the American Institute of Aeronautics and Astronautics, and the Society of Photo-Optical Instrumentation Engineers. He has published numerous papers in the control systems field and holds two patents.

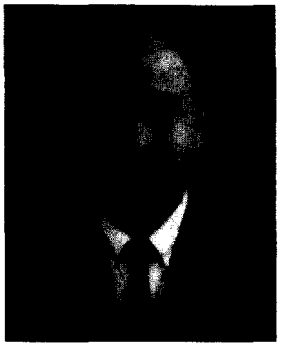

**Jafar Saniie** (S'80—M'81—SM'91) was born in Iran on March 21, 1952. He received his B.S. in electrical engineering from the University of Maryland, College Park, in 1974. In 1977, he received an M.S. in biomedical engineering from Case Western Reserve University, and, in 1981, a Ph.D. in electrical engineering from Purdue University, Lafayette, IN.

In 1981, he joined the Applied Physics Laboratory, University of Helsinki, Finland to conduct research in photothermal and photoacoustic imaging. Since 1983, Dr. Saniie has been with the Department of Electrical and Computer Engineering, Illinois Institute of Technology, Chicago, where he is Professor and Director of the Ultrasonic Information Processing Laboratory. His current research activities include radar signal processing, estimation and detection, ultrasonic medical imaging, computer tomography, nondestructive testing, and digital hardware design.

Dr. Saniie is a technical committee member of the IEEE Ultrasonics Symposium, and editorial advisory member of the *Nondestructive Testing and Evaluation Journal*. He is a member of Sigma Xi, Tau Beta Pi, Eta Kappa Nu, and has served as IEEE Branch Counselor (1984–1990). He is the 1986 recipient of the outstanding IEEE Student Counselor Award.